

## Effect of Nd content on electrochemical performances of nanocrystalline and amorphous $(\text{Mg}_{24}\text{Ni}_{10}\text{Cu}_2)_{100-x}\text{Nd}_x$ ( $x=0-20$ ) alloys prepared by melt spinning

Yang-huan ZHANG<sup>1,2</sup>, Tai YANG<sup>2</sup>, Wen-gang BU<sup>1,2</sup>, Ying CAI<sup>1</sup>, Guo-fang ZHANG<sup>1</sup>, Dong-liang ZHAO<sup>2</sup>

1. Key Laboratory of Integrated Exploitation of Baiyun Obo Multi-Metal Resources,  
Inner Mongolia University of Science and Technology, Baotou 014010, China;

2. Department of Functional Material Research, Central Iron and Steel Research Institute, Beijing 100081, China

Received 12 September 2013; accepted 21 October 2013

**Abstract:** The nanocrystalline and amorphous  $\text{Mg}_2\text{Ni}$ -type alloys with a chemical composition of  $(\text{Mg}_{24}\text{Ni}_{10}\text{Cu}_2)_{100-x}\text{Nd}_x$  ( $x=0, 5, 10, 15, 20$ ) were fabricated by melt spinning technology. The effects of spinning rate on the structure and electrochemical hydrogen storage performance of the alloys were investigated. The as-spun Nd-free alloy displays an entire nanocrystalline structure, whereas the as-spun Nd-added alloys hold a nanocrystalline and amorphous structure, suggesting that the addition of Nd facilitates the glass forming of the  $\text{Mg}_2\text{Ni}$ -type alloys. Increasing the spinning rate from 0 to 40 m/s gives rise to the discharge capacity growing from 42.5 to 100.6 mA·h/g for the  $x=0$  alloy and from 86.4 to 452.8 mA·h/g for the  $x=10$  alloy. And the cycle stability ( $S_{20}$ ) rises from 40.2% to 41.1% for the  $x=0$  alloy and from 53.2% to 89.7% for the  $x=10$  alloy, respectively.

**Key words:** hydrogen storage; alloy;  $\text{Mg}_2\text{Ni}$ -type alloy; Nd; melt spinning; structure

### 1 Introduction

$\text{Mg}_2\text{Ni}$ -type metallic hydrides are looked upon as one of the most promising hydrogen storage materials applied in hydrogen fuel cell vehicle or negative electrodes in Ni–MH batteries [1] because of their major advantages, such as the high gaseous hydrogen absorption capacity (3.6% in mass fraction) for  $\text{Mg}_2\text{NiH}_4$  and the large gravimetric capacity (about 1000 mA·h/g) [2,3]. However, some innate shortcomings, such as relatively high H-desorption temperature, sluggish hydriding/dehydriding kinetics and extremely poor electrochemical cycle stability, make the attempt of the practical application of the alloys frustrated seriously. In spite of facing huge challenges, the researchers in this field still persist in the firm confidence to improve the properties of the alloys and achieve a series of important progress.

It is universally agreed that alloying and microstructure modification are the effective approaches for improving the hydriding properties [4]. Particularly, the partial substitution of some elements (Y, La, Cu, Fe,

V, Cr, Co, Zr) for Ni in  $\text{Mg}_2\text{Ni}$  alloy makes the stability of the hydride decrease and the hydrogen desorption reaction easier [5–7], and thus substitution can effectively prevent the alloy from being corroded, so as to improve the cycle stability [8,9]. Furthermore, it was verified that the hydriding and dehydriding kinetics of the Mg and Mg based alloys are very sensitive to their structures [10,11]. In particular, the as-milled Mg–Ni based alloys with nanocrystalline and amorphous structure can react with hydrogen even at room temperature [12] and can electrochemically absorb and desorb large amount of hydrogen at room temperature [13,14].

High energy ball-milling (HEBM) has inarguably been considered to be quite an effective method for fabricating nanocrystalline and amorphous Mg and Mg-based alloys [15]. However, the cycle stabilities of the milled Mg and Mg-based alloys are very poor owing to the vanishment of the metastable structures generated by ball milling during the multiple hydrogen absorbing and desorbing cycles [16]. Alternatively, the melt-spinning technique is also a useful method to obtain an amorphous and/or nanocrystalline structure in the

absence of disadvantages inherent to the ball milling process. It was ascertained that the Mg-based alloys with nanocrystalline and amorphous structure produced by melt-spinning exhibit excellent hydriding characteristics, similar to the alloys produced by the HEBM [17]. Also, the microstructure created by melt spinning displays a much higher stability during the hydrogen absorbing and desorbing cycles compared with the microstructure generated by HEBM [18,19].

Our previous investigations have found that the substitution of La for Mg and M (M=Co, Cu, Mn) for Ni improved the electrochemical and gaseous hydrogen storage performances of the Mg<sub>2</sub>Ni-type alloys dramatically [20–23]. Therefore, it is expected that the joint addition of Cu and Nd combining with a proper melt spinning technique may ameliorate the electrochemical hydrogen storage performance of the Mg<sub>2</sub>Ni-type alloys more strikingly. To validate this, a systematical investigation about the effects of melt spinning on the structures and electrochemical hydrogen storage performances of the (Mg<sub>24</sub>Ni<sub>10</sub>Cu<sub>2</sub>)<sub>100-x</sub>Nd<sub>x</sub> (x=0–20) electrode alloys was performed, and some experimental results were provided.

## 2 Experimental

The compositions of the experimental alloys were (Mg<sub>24</sub>Ni<sub>10</sub>Cu<sub>2</sub>)<sub>100-x</sub>Nd<sub>x</sub> (x=0, 5, 10, 15, 20). For convenience, the alloys were denoted with Nd content as Nd<sub>0</sub>, Nd<sub>5</sub>, Nd<sub>10</sub>, Nd<sub>15</sub> and Nd<sub>20</sub>, respectively. The alloy ingots were prepared by using a vacuum induction furnace in a helium atmosphere at a pressure of 0.04 MPa to prevent Mg from volatilizing. A part of the as-cast alloys were re-melted and spun by melt spinning with a rotating copper roller cooled by water. The spinning rates used in the experiment were 10, 20, 30 and 40 m/s, respectively, which were approximately expressed by the linear velocity of the copper roller.

The phase structures of the as-cast and spun alloys were determined by X-ray diffraction (XRD) (D/max/2400). The diffraction, with the experimental parameters of 160 mA, 40 kV and 10 (°)/min respectively, was performed with Cu K<sub>α1</sub> radiation filtered by graphite.

A Philips SEM (QUANTA 400) linked with an energy dispersive spectrometer (EDS) was used for morphological characterization and chemical composition analysis of the as-cast alloys.

The thin film samples of the as-spun alloys prepared by ion etching technology were observed by high resolution transmission electron microscope (HRTEM) (JEM–2100F, operated at 200 kV) and their crystalline states were ascertained by selected area electron diffraction (SAED).

The alloys were pulverized by mechanical milling

into fine powder with a diameter of 35 μm, and then mixing the alloy powder with carbonyl nickel powder in a mass ratio of 1:4. The mixture was cold pressed under a pressure of 35 MPa into round electrode pellet with 15 mm in diameter whose total mass was 1 g. The electrochemical measurements were performed at 30 °C with a tri-electrode open cell consisting of a working electrode (the metal hydride electrode), a sintered Ni(OH)<sub>2</sub>/NiOOH counter electrode as well as a Hg/HgO reference electrode, which were immersed in 6 mol/L KOH electrolyte. The voltage between the negative electrode and the reference one was defined as the discharge voltage. In every cycle, the alloy electrode was first charged with a constant current density, after resting for 15 min, it was discharged at the same current density to cut-off voltage of –0.500 V.

## 3 Results and discussion

### 3.1 Microstructure characteristics

The phase components and structure characteristics of the as-cast and spun (Mg<sub>24</sub>Ni<sub>10</sub>Cu<sub>2</sub>)<sub>100-x</sub>Nd<sub>x</sub> (x=0–20) alloys are also subjected to XRD analysis, as demonstrated in Fig. 1. It is evident that the as-cast and spun Nd<sub>0</sub> alloys display a typical crystalline structure. The melt spinning incurs the diffraction peaks of the Nd<sub>0</sub> alloy evidently broadened, to be put down to the significant refinement of the grain. Interestingly, the as-spun Nd<sub>20</sub> alloy exhibits an obvious amorphous structure and the degree of amorphization evidently heightens with the spinning rate rising, suggesting that the addition of Nd facilitates the glass forming in the Mg<sub>2</sub>Ni-type alloys. Moreover, a comparison of Figs. 1(a) with (b) finds that the addition of Nd gives rise to the formation of the secondary phases Nd<sub>5</sub>Mg<sub>41</sub> and NdNi in the as-cast alloy without altering the Mg<sub>2</sub>Ni major phase.

TEM micrographs as well as SAED patterns of the as-spun (30 m/s) (Mg<sub>24</sub>Ni<sub>10</sub>Cu<sub>2</sub>)<sub>100-x</sub>Nd<sub>x</sub> (x=0–20) alloys are shown in Fig. 2, from which it can be seen that the as-spun Nd<sub>0</sub> alloy exhibits an entire nanocrystalline structure with a mean grain size of about 5 nm, and its SAED pattern appears sharp multi-haloes, corresponding to a crystalline structure. Some crystal defects such as subgrains and grain boundaries can be seen clearly. Nevertheless, the as-spun Nd<sub>20</sub> alloy differing from Nd<sub>0</sub> alloy displays a clear feature of the amorphous structure, and its electron diffraction pattern consists of broad and dull halo, indicating the existence of an amorphous structure, which conforms well to the XRD observations as depicted in Fig. 1. Meanwhile, the phase components of the as-cast (Mg<sub>24</sub>Ni<sub>10</sub>Cu<sub>2</sub>)<sub>100-x</sub>Nd<sub>x</sub> (x=0–20) alloys were analyzed by SEM linked with EDS, and the representative morphologies and EDS patterns of the alloys are illustrated in Fig. 3. It was noted that the

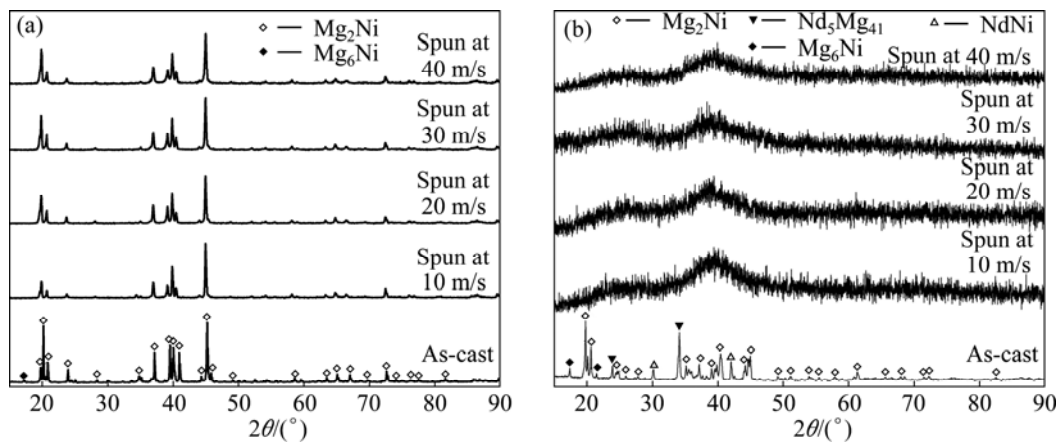


Fig. 1 XRD patterns of as-cast and spun  $\text{Nd}_0$  and  $\text{Nd}_{20}$  alloys: (a)  $\text{Nd}_0$  alloy; (b)  $\text{Nd}_{20}$  alloy

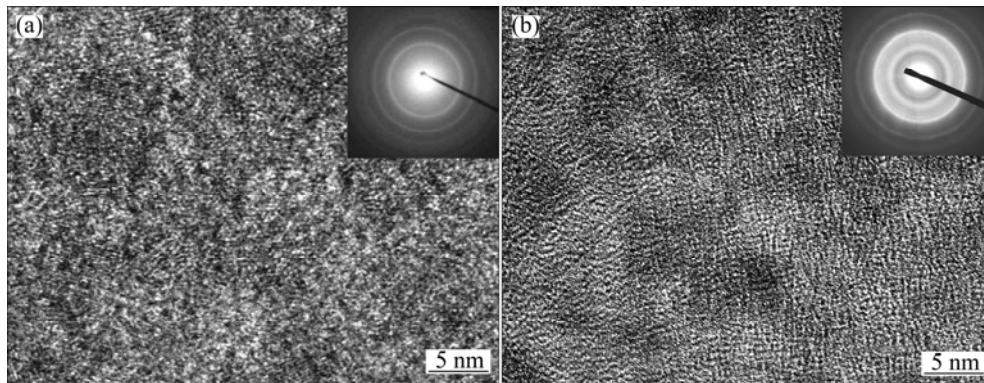


Fig. 2 HRTEM images and SAED patterns of as-spun (at 40 m/s)  $(\text{Mg}_{24}\text{Ni}_{10}\text{Cu}_2)_{100-x}\text{Nd}_x$  ( $x=0-20$ ) alloys: (a)  $\text{Nd}_0$ ; (b)  $\text{Nd}_{20}$

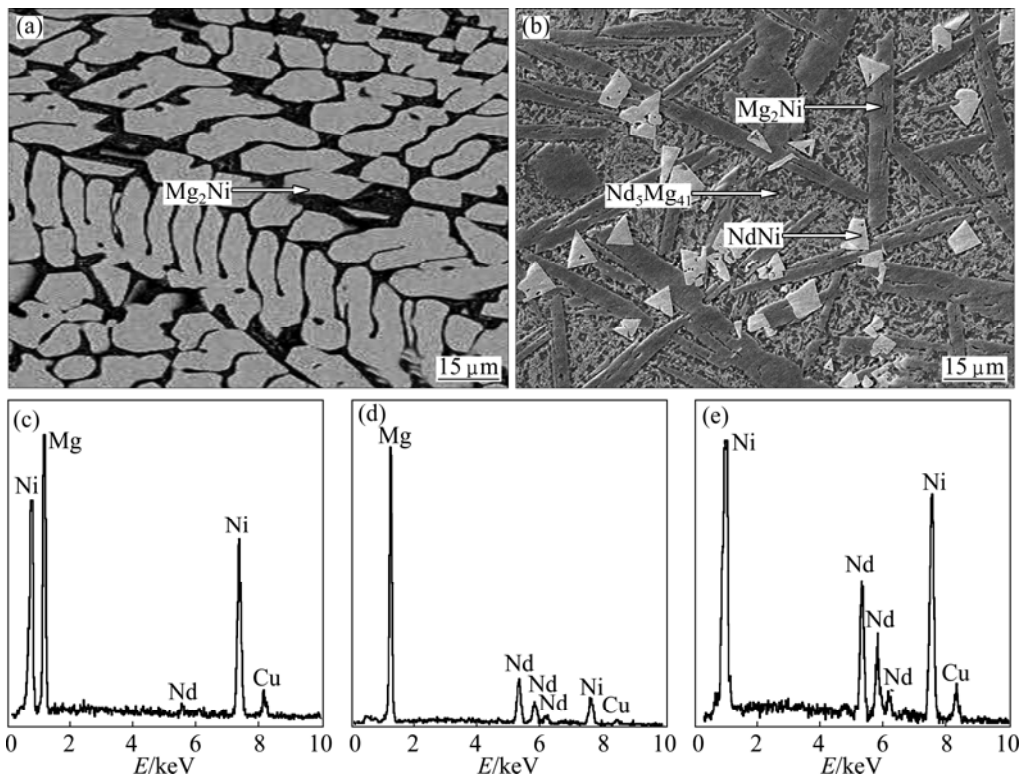


Fig. 3 SEM images (a, b) together with typical EDS spectra (c, d, e) of as-cast  $(\text{Mg}_{24}\text{Ni}_{10}\text{Cu}_2)_{100-x}\text{Nd}_x$  ( $x=0-20$ ) alloys: (a)  $\text{Nd}_0$ ; (b)  $\text{Nd}_{20}$ ; (c)  $\text{Mg}_2\text{Ni}$ ; (d)  $\text{Nd}_5\text{Mg}_{41}$ ; (e)  $\text{NdNi}$

addition of Nd brings on a dramatic variation in the morphologies of the as-cast alloys. The as-cast Nd<sub>0</sub> alloy shows a typical dendritic structure, but it disappears completely and some secondary phases appear when the amount of the Nd added is  $x=20$ . The EDS patterns reveal that the Nd<sub>20</sub> alloy is of a multiphase structure, containing major phase Mg<sub>2</sub>Ni and the secondary phases Nd<sub>5</sub>Mg<sub>41</sub> and NdNi, which agrees well with the result of the XRD detection.

### 3.2 Electrochemical hydrogen storage performance

#### 3.2.1 Activation ability, discharge potential and discharge capacity

The activation process of an alloy electrode is the course that the discharge capacity of the alloy gradually grows to the maximum value through charge/discharge cycles at a constant current density. The activation capability was characterized by the cycle number ( $n$ ) required for attaining the greatest discharge capacity at a constant current density. It is quite clear that the smaller the  $n$  is, the better the activation capability will be. The activation capabilities of the alloys are inspected by constituting the relationship between the discharge capacity and the cycle number, as provided in Fig. 4. It is

noted that the as-cast and spun alloys can reach their maximum discharge capacity at most three charging/discharging cycles, displaying superior activation capability. Figure 5 presents the variations of the discharge potential of the as-cast and spun Nd<sub>0</sub> and Nd<sub>20</sub> alloys with the discharge capacity. Apparently, the discharge potentials of the alloy electrodes drop in varying degree with the discharge carrying out, meaning that the output power of the battery is unstable. Evidently, the discharge potential characteristic being directly associated with the stability of the output power is an extremely important performance of the alloy electrode, which is characterized by the potential plateau of the discharge curves of the alloys. The longer and the more horizontal the discharge potential plateau is, the better the discharge potential characteristics of the alloy will be. Here, it is noted that discharge curves have the different width of the discharge potential plateau based on the oxidation of desorbed hydrogen from the hydride. The melt spinning greatly modifies discharge potential characteristics of the Nd<sub>0</sub> and Nd<sub>20</sub> alloys, making discharge potential rise and the discharge plateau extend. Furthermore, it can be found that the melt spinning makes a positive contribution to the potential

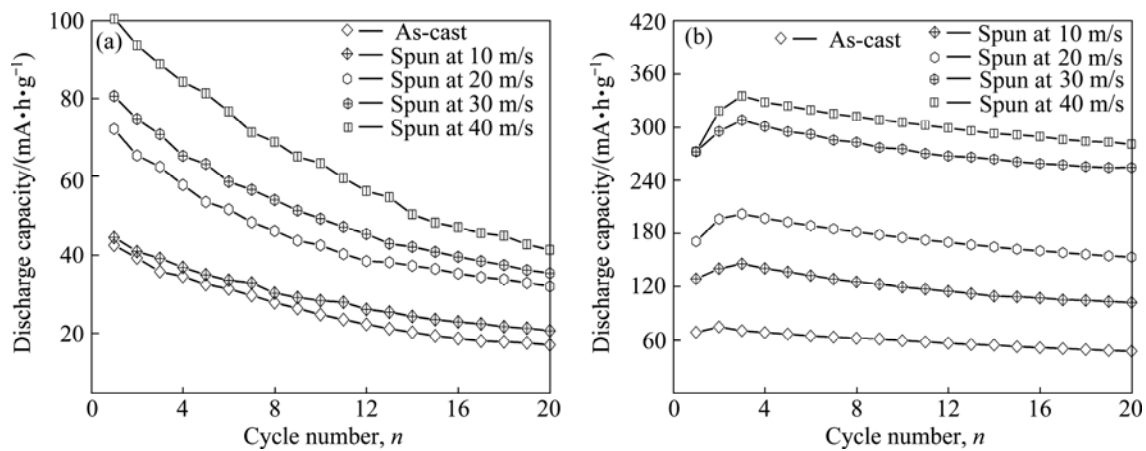


Fig. 4 Evolution of discharge capacities of as-cast and spun alloys with cycle number: (a) Nd<sub>0</sub> alloy; (b) Nd<sub>20</sub> alloy

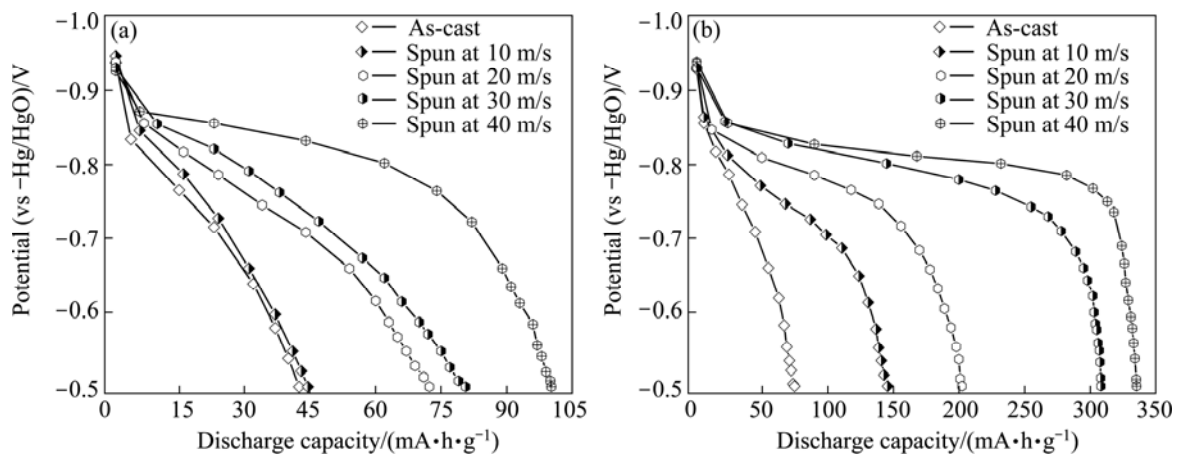


Fig. 5 Discharge potential curves of as-cast and spun alloys: (a) Nd<sub>0</sub> alloy; (b) Nd<sub>20</sub> alloy

characteristics of the Nd<sub>20</sub> alloy more conspicuously compared with the Nd<sub>0</sub> alloy, for which the glass forming facilitated by Nd adding is principally responsible. Furthermore, it is found that, besides improving potential characteristic, the melt spinning also enhances the discharge capacity of alloys dramatically. As described in Fig. 6, the discharge capacities of the alloys always mount up with the spinning rate growing. Increasing the spinning rate from 0 to 40 m/s results in the growing of the discharge capacity from 42.5 to 100.6 mA·h/g for the Nd<sub>0</sub> alloy and from 86.4 to 452.8 mA·h/g for the Nd<sub>10</sub> alloy, respectively.

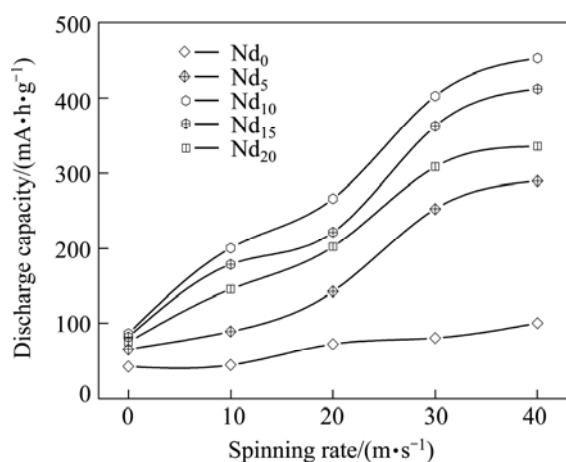


Fig. 6 Evolution of discharge capacity of alloys with spinning rate varying

The observed variations in the electrochemical properties of the alloys incurred by melt spinning may be associated with the differences in their microstructures. In terms of the excellent activation property, it is considered to be ascribed to the multiphase structure in the as-cast alloy or nanocrystalline structure in the as-spun alloy. It is known to all that the activation capability of an alloy electrode is closely related with the change of the internal energy of the hydride system before and after hydrogen absorption. The larger the additive internal energy is, the poorer the activation performance of the alloy will be [10]. In general, the internal energy involves both the surface energy and the strain energy. The former originates from oxidation film forming on the surface of the electrode alloy, and the latter is generated by hydrogen atoms entering the tetrahedral or octahedral lattice interstitial position. For the as-cast alloys, the superior activation performance is ascribed to multiphase structure due to the phase boundary providing good tunnels for hydrogen atoms to diffuse, further improving the activation capability [24,25]. And in respect of the as-spun alloys, it is ascribed to the nanocrystalline/amorphous structure generated by melt spinning because numerous grain

boundaries probably act as buffer areas which can greatly release the lattice distortion and strain energy accumulated during hydrogen absorption process. The positive contribution of the melt spinning to the discharge capacity of the alloys is most likely associated with the microstructures changed by melt spinning. The crystalline material, when melt spun, becomes at least partially disordered and its structure changes into nanocrystalline or amorphous, as presented in Fig. 2. As a result, a large number of interfaces and grain boundaries are created in the nanocrystalline materials, which make a positive contribution to the discharge capacity due to the grain boundaries possessing the distribution of the maximum hydrogen concentrations [26]. In addition, such a nanocrystalline structure greatly facilitates to ameliorate the hydriding and dehydriding ability of Mg<sub>2</sub>Ni-type alloys [27]. With respect to the reason why the positive contribution produced by melt spinning to the discharge capacity of the Nd-added alloy is more pronounced than that of Nd-free alloy, it is considered to be due to the increased glass forming ability promoted by Nd adding because an adequate proportion of amorphous and nanocrystalline in Mg–Ni-based alloy possesses superior discharge property [28].

### 3.2.2 Cycle stability

Cycle stability, one of the major properties which are adopted to evaluate whether or not a kind of an alloy can be applied as a negative electrode material of Ni–MH battery, is symbolized by the capacity retaining rate ( $S_n$ ), which is defined as  $S_n = C_n / C_{max} \times 100\%$ , where  $C_{max}$  is the maximum discharge capacity and  $C_n$  is the discharge capacity at the  $n$ th charge-discharge cycle, respectively. Apparently, it means that the larger the capacity retaining rate ( $S_n$ ) is, the better the cycle stability of the alloy will be. The variations of the  $S_n$  values of the as-cast and spun Nd<sub>0</sub> and Nd<sub>20</sub> alloys depending on the cycle numbers are demonstrated in Fig. 7, from which the degradation process of the discharge capacity of the alloys can be seen clearly. The slopes of the curves qualitatively reflect the degradation rate of the discharge capacity during the charging–discharging cycle, namely the smaller the slope of the curve is, the better the cycle life of the alloy will be. Evidently, the melt spinning makes little impact on the capacity retention rate of the Nd<sub>0</sub> alloy but remarkable effect on the Nd<sub>20</sub> alloy, namely the  $S_n$  value of the Nd<sub>20</sub> alloy dramatically grows with the spinning rate rising. In order to directly display the effect of the spinning rate on the cycle stability of the alloy, here we provide the variations of the  $S_{20}$  values of the alloys at the 20th cycle with spinning rate, as illustrated in Fig. 8. It is found that

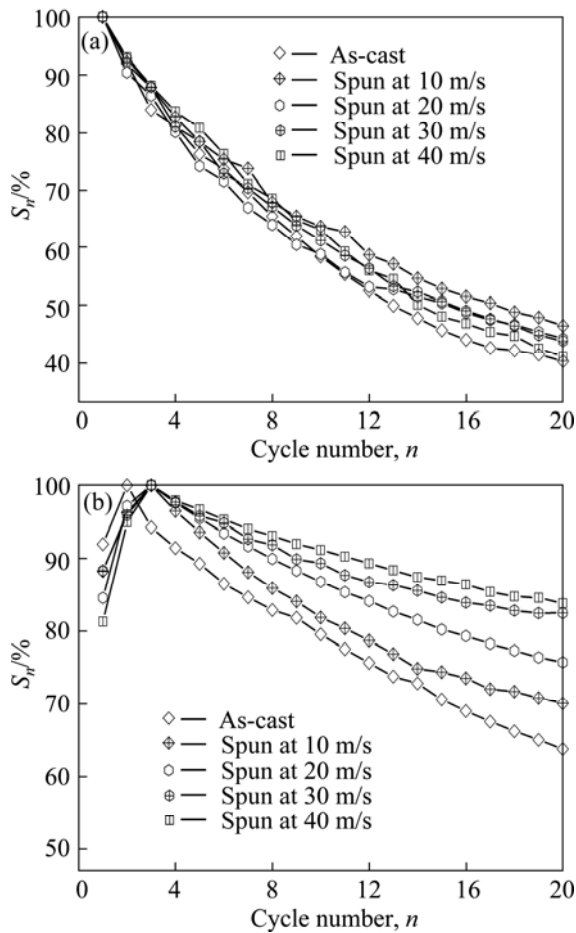


**Fig. 7** Evolution of capacity retaining rates ( $S_n$ ) of as-cast and spun alloys with cycle number: (a)  $Nd_0$  alloy; (b)  $Nd_{20}$  alloy

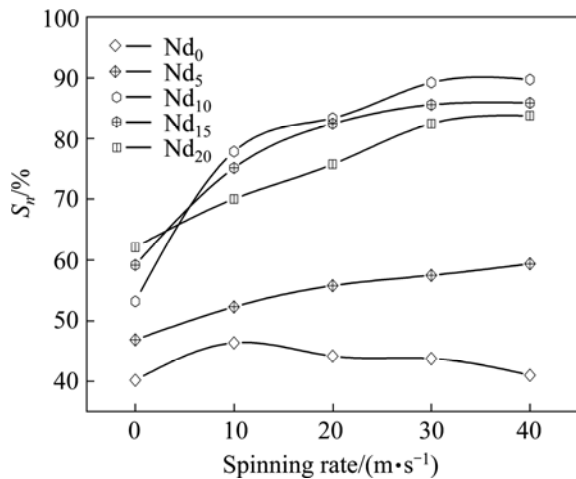


**Fig. 8** Evolution of  $S_{20}$  values of as-cast and spun  $(Mg_{24}Ni_{10}Cu_2)_{100-x}Nd_x$  ( $x=0-20$ ) alloys with Nd content varying

the melt spinning engenders different impacts on the cycle stabilities of the Nd-free and Nd-added alloys. The  $S_n$  values of the Nd-added alloys clearly augment with the rising of the spinning rate, whereas the  $Nd_0$  alloy

alters a little in the same condition. Particularly, the growing of the spinning rate from 0 to 40 m/s brings on an augment of the  $S_{20}$  value from 40.2% to 46.4% (10 m/s) and then to 41.1% for the  $Nd_0$  alloy and from 53.2% to 89.7% for the  $Nd_{10}$  alloy, respectively.

Here, some acceptable interpretations are provided as reasons for the ameliorated cycle stability by melt spinning. It has been ascertained that the sharp degradation of the discharge capacity of  $Mg_2Ni$  alloy during the charge–discharge cycling is caused by forming and thickening of  $Mg(OH)_2$  surface layer, which hinders the hydrogen atoms from diffusing in or out, in alkaline solution [29]. Moreover, the hydrogen storage material suffers an inevitable volume change during the charge–discharge process which aggravates the alloy’s cracking and pulverizing and then makes the surface of the material apt to be oxidized, which is also supported by our experimental result, as provided in Fig. 9. The alloy particles (denoted as *A*) with a size of about 30  $\mu m$  and ultrafine Ni powders appearing in an aggregation sate (denoted as *B*) can be seen clearly. Furthermore, it is evident that there are numerous cracks on the surfaces of the alloy particles after electrochemical cycle, but the sizes of the alloy particles have no obvious change, indicating that the pulverization of alloy particles takes place scarcely in the process of the electrochemical cycle. Noticeably, the alloy particles after cycling are covered by a rough and gossypine layer, which is inspected by XRD to be  $Mg(OH)_2$ , as demonstrated in Fig. 10. Evidently, it is noted that the thickness of the covering layer on the surface of the  $Nd_{20}$  alloy particle is much less than that of the  $Nd_0$ , indicating that the addition of Nd can significantly enhance the anti-corrosion and anti-oxidation ability of the  $Mg_2Ni$  alloy, which was also reported by TERESIAK et al [13]. Besides, it is very evident that the cracks on the surface of the  $Nd_{20}$  alloy particle after cycling are much fewer than that of the  $Nd_0$  one, suggesting that the addition of Nd can markedly improve the anti-pulverization ability. The above-mentioned actions of Nd adding are considered to be ascribed to two aspects. Firstly, the addition of rare elements (La, Nd, Sm, Y) results in a significant enlargement of the cell volume of the  $Mg_2Ni$  alloy, decreasing the ratios of expansion/contraction in the process of hydrogen absorption/desorption, thus increasing the anti-pulverization capability. Secondly, the facilitated glass forming by Nd adding is extremely important because an amorphous phase improves not only anti-pulverization ability but also anti-corrosion and anti-oxidation abilities of the alloy electrode in a corrosive electrolyte [30]. As a matter of fact, the melt spinning makes a more significantly positive contribution to the cycle stability of the Nd-added alloys

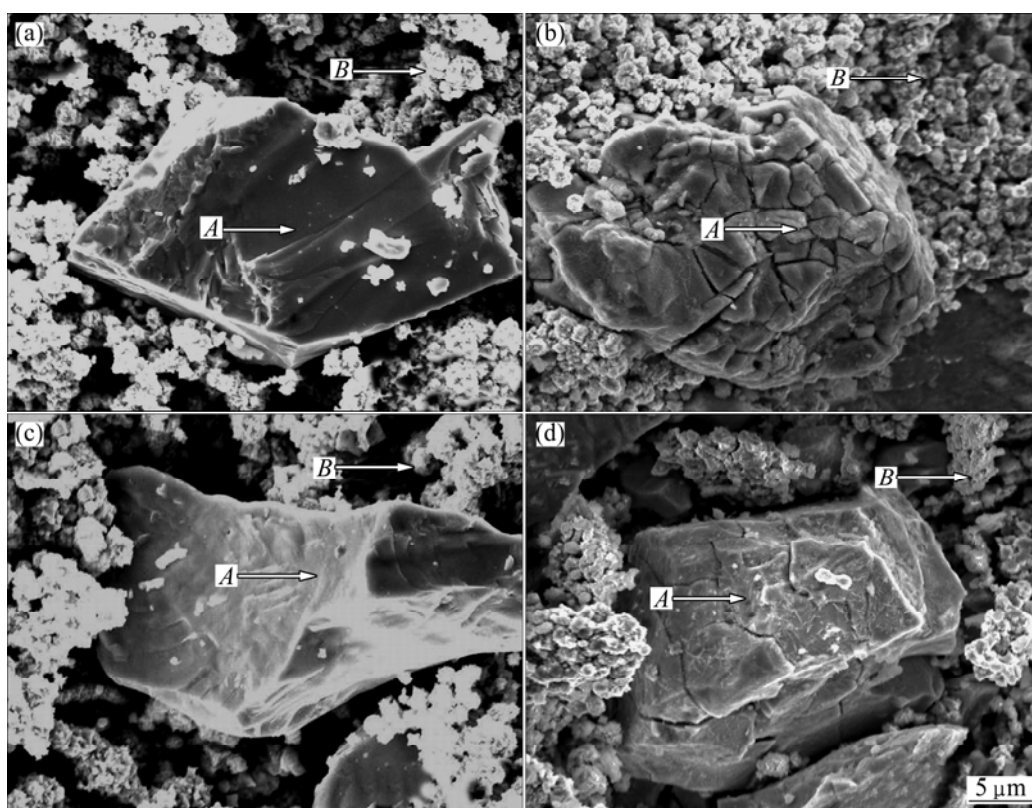


Fig. 9 SEM images of as-spun (40 m/s) Nd<sub>0</sub> (a, b) and Nd<sub>20</sub> (c, d) alloys before (a, c) and after (b, d) electrochemical cycle

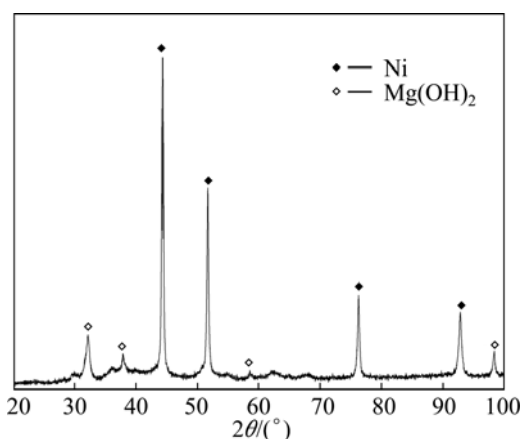


Fig. 10 XRD pattern of as-cast Nd<sub>0</sub> alloy after electrochemical cycle

compared with the Nd-free alloy, which is most likely related to their different structures. The entire nanocrystalline of the Nd<sub>0</sub> alloy formed by melt spinning is considered to be detrimental for corrosion in the electrolyte during cycling due to inevitable intercrystalline corrosion [31]. Quite the contrary, the amorphous structure of the Nd<sub>20</sub> alloy is extremely beneficial for improving its corrosion resistance. Based on the above-mentioned causes, it is very easy to understand why the Nd-added alloys display much higher cycle stability than the Nd-free alloy.

## 4 Conclusions

1) The inspection of the structures reveals that the addition of Nd facilitates the glass forming in the Mg<sub>2</sub>Ni alloys. As a result, the as-spun Nd-free alloy displays an entire nanocrystalline structure, whereas the as-spun Nd-added alloy obviously shows an amorphous structure.

2) The melt spinning makes a positive contribution to the electrochemical performances of the alloys, including discharge capacity, potential characteristic and cycle stability, and its effects on the electrochemical performances of the Nd-added alloys are much more significant than those of the Nd-free alloy, for which the different structures generated by melt spinning are principally responsible.

3) Furthermore, the addition of Nd obviously enhances the anti-corrosion and anti-pulverization ability of the alloy, which is viewed as the root reason why the cycle stability of Nd-added alloys is much superior to that of the Nd-free one.

## References

- [1] ORIMO S, FUJII H. Effects of nanometer-scale structure on hydriding properties of Mg–Ni alloys: A review [J]. *Intermetallics*, 1998, 6(3): 185–192.
- [2] JAIN I P, LAL C, JAIN A. Hydrogen storage in Mg: A most

- promising material [J]. *International Journal of Hydrogen Energy*, 2010, 35(10): 5133–5144.
- [3] SCHLAPBACH L, ZÜTTEL A. Hydrogen-storage materials for mobile applications [J]. *Nature*, 2001, 414: 353–358.
- [4] SPASSOV T, LYUBENOVA L, KÖSTER U, BARÓ M D. Mg–Ni–RE nanocrystalline alloys for hydrogen storage [J]. *Materials Science and Engineering A*, 2004, 375–377: 794–799.
- [5] WOO J H, LEE K S. Electrode characteristics of nanostructured Mg<sub>2</sub>Ni-type alloys prepared by mechanical alloying [J]. *Journal of the Electrochemical Society*, 1999, 146(3): 819–823.
- [6] ZHANG Y H, ZHAO D L, LI B W, MA Z H, GUO S H, WANG X L. Influence of substituting Ni with Co on hydriding and dehydriding kinetics of melt spun nanocrystalline and amorphous Mg<sub>2</sub>Ni-type alloys [J]. *Journal of Central South University of Technology*, 2011, 18(2): 303–309.
- [7] ZHANG Yang-huan, MA Zhi-hong, ZHAO Dong-liang, ZHANG Yin, GUO Shi-hai, WANG Xin-lin. Influences of substituting Ni with Co on structure and electrochemical hydrogen storage characteristics of melt spun Mg<sub>2</sub>Ni-type alloys [J]. *The Chinese Journal of Nonferrous Metals*, 2011, 21(1): 118–124. (in Chinese)
- [8] GOO N H, JEONG W T, LEE K S. Effects of Zr addition on discharge properties of mechanically alloyed Mg<sub>2</sub>Ni hydrogen-storage alloy electrode [J]. *Journal of Power Sources*, 2000, 87(1–2): 118–124.
- [9] ANIK M. Improvement of the electrochemical hydrogen storage performance of Mg<sub>2</sub>Ni by the partial replacements of Mg by Al, Ti and Zr [J]. *Journal of Alloys and Compounds*, 2009, 486(1–2): 109–114.
- [10] WU M S, WU H R, WANG Y Y, WAN C C. Surface treatment for hydrogen storage alloy of nickel/metal hydride battery [J]. *Journal of Alloys and Compounds*, 2000, 302(1–2): 248–257.
- [11] ZHANG Y H, ZHAO D L, LI B W, QI Y, GUO S H, WANG X L. Hydrogen storage behaviours of nanocrystalline and amorphous Mg<sub>20</sub>Ni<sub>10-x</sub>Co<sub>x</sub> (x=0–4) alloys prepared by melt spinning [J]. *Transactions of Nonferrous Metals Society of China*, 2010, 20(3): 405–411.
- [12] SAKINTUNA B, LAMARI-DARKRIM F, HIRSCHER M. Metal hydride materials for solid hydrogen storage: A review [J]. *International Journal of Hydrogen Energy*, 2007, 32(9): 1121–1140.
- [13] TERESIAK A, GEBERT A, SAVYAK M, UHLEMANN M, MICKEL C, MATTERN N. In situ high temperature XRD studies of the thermal behaviour of the rapidly quenched Mg<sub>77</sub>Ni<sub>18</sub>Y<sub>5</sub> alloy under hydrogen [J]. *Journal of Alloys and Compounds*, 2005, 398(1–2): 156–164.
- [14] ZHANG Y H, LI B W, REN H P, HOU Z H, HU F, WANG X L. Influences of melt spinning on electrochemical hydrogen storage performance of nanocrystalline and amorphous Mg<sub>2</sub>Ni-type alloys [J]. *Journal of Central South University of Technology*, 2011, 18(6): 1825–1832.
- [15] RONGEAT C, ROUÉ L. Effect of particle size on the electrode performance of MgNi hydrogen storage alloy [J]. *Journal of Power Sources*, 2004, 132(1–2): 302–308.
- [16] SONG M Y, KWON S N, BAE J S, HONG S H. Hydrogen-storage properties of Mg–23.5Ni–(0 and 5)Cu prepared by melt spinning and crystallization heat treatment [J]. *International Journal of Hydrogen Energy*, 2008, 33(6): 1711–1718.
- [17] TODOROVA S, SPASSOV T. Mg<sub>6</sub>Ni formation in rapidly quenched amorphous Mg–Ni alloys [J]. *Journal of Alloys and Compounds*, 2009, 469(1–2): 193–196.
- [18] LIANG G Y, WU D C, LI L, HUANG L J. A discussion on decay of discharge capacity for amorphous Mg–Ni–Nd hydrogen storage alloy [J]. *Journal of Power Sources*, 2009, 186(2): 528–531.
- [19] ZHANG Y H, LÜ K, ZHAO D L, GUO S H, QI Y, WANG X L. Electrochemical hydrogen storage characteristics of nanocrystalline and amorphous Mg<sub>2</sub>Ni-type alloys prepared by melt-spinning [J]. *Transactions of Nonferrous Metals Society of China*, 2011, 21(3): 502–511.
- [20] ZHANG Y H, ZHAO D L, LI B W, GUO S H, QI Y, WANG X L. Influence of rapid quenching on hydrogen storage characteristics of nanocrystalline Mg<sub>2</sub>Ni-type alloys [J]. *Transactions of Nonferrous Metals Society of China*, 2010, 20(8): 1439–1446.
- [21] ZHANG Y H, SONG C H, REN H P, LI Z G, HU F, ZHAO D L. Enhanced hydrogen storage kinetics of nanocrystalline and amorphous Mg<sub>2</sub>Ni-type alloy by substituting Ni with Co [J]. *Transactions of Nonferrous Metals Society of China*, 2011, 21(9): 2002–2009.
- [22] ZHANG Y H, QI Y, REN H P, MA Z H, GUO S H, ZHAO D L. Hydriding and dehydriding kinetics of nanocrystalline and amorphous Mg<sub>2</sub>Ni<sub>1-x</sub>Mn<sub>x</sub> (x=0–0.4) alloys prepared by melt spinning [J]. *Journal of Central South University of Technology*, 2011, 18(4): 985–992.
- [23] ZHANG Yang-huan, ZHANG Guo-fang, LI Xia, HOU Zhong-hui, REN Hui-ping, ZHAO Dong-liang. Structure and hydrogen storage kinetics of as-spun Mg<sub>2</sub>Ni type alloys [J]. *Journal of Central South University: Science and Technology*, 2012, 43(6): 2101–2107. (in Chinese)
- [24] XIE D H, LI P, ZENG C X, SUN J W, QU X H. Effect of substitution of Nd for Mg on the hydrogen storage properties of Mg<sub>2</sub>Ni alloy [J]. *Journal of Alloys and Compounds*, 2009, 478(1–2): 96–102.
- [25] ZHANG Y H, ZHAO D L, DONG X P, QI Y, GUO S H, WANG X L. Effects of rapid quenching on structure and electrochemical characteristics of La<sub>0.5</sub>Ce<sub>0.2</sub>Mg<sub>0.3</sub>Co<sub>0.4</sub>Ni<sub>2.6-x</sub>Mn<sub>x</sub> (x=0–0.4) electrode alloys [J]. *Transactions of Nonferrous Metals Society of China*, 2009, 19(2): 364–371.
- [26] ORIMO S, FUJII H. Materials science of Mg–Ni-based new hydrides [J]. *Applied Physics A*, 2001, 72(2): 167–186.
- [27] KUMARA L H, VISWANATHAN B, MURTHY S S. Hydrogen absorption by Mg<sub>2</sub>Ni prepared by polyol reduction [J]. *Journal of Alloys and Compounds*, 2008, 461(1–2): 72–76.
- [28] SPASSOV T, KÖSTER U. Hydrogenation of amorphous and nanocrystalline Mg-based alloys [J]. *Journal of Alloys and Compounds*, 1999, 287(1–2): 243–250.
- [29] DORNHEIM M, DOPPIU S, BARKHORDARIAN G, BOESENBERG U, KLASSEN T, GUTFLEISCH O, BORMANN R. Hydrogen storage in magnesium-based hydrides and hydride composites [J]. *Scripta Materialia*, 2007, 56(10): 841–846.
- [30] ZHANG Y H, ZHAO D L, SHI Y C, QI Y, GUO S H, WANG X L. Structures and electrochemical performances of La<sub>0.75-x</sub>Zr<sub>x</sub>Mg<sub>0.25</sub>Ni<sub>3.2</sub>Co<sub>0.2</sub>Al<sub>0.1</sub> (x=0–0.2) electrode alloys prepared by melt spinning [J]. *Transactions of Nonferrous Metals Society of China*, 2010, 20(4): 607–613.
- [31] SIMIČIĆ M V, ZDUJIC M, DIMITRIJEVIĆ R, NIKOLIĆ-BUJANOVIĆ L, POPOVIĆ N H. Hydrogen absorption and electrochemical properties of Mg<sub>2</sub>Ni-type alloys synthesized by mechanical alloying [J]. *Journal of Power Sources*, 2006, 158(1): 730–734.

# Nd 含量对快淬纳米晶和非晶 (Mg<sub>24</sub>Ni<sub>10</sub>Cu<sub>2</sub>)<sub>100-x</sub>Nd<sub>x</sub> (x=0~20)合金电化学性能的影响

张羊换<sup>1,2</sup>, 杨泰<sup>2</sup>, 卜文刚<sup>1,2</sup>, 蔡颖<sup>1</sup>, 张国芳<sup>1</sup>, 赵栋梁<sup>2</sup>

1. 内蒙古科技大学 内蒙古自治区白云鄂博矿多金属资源综合利用重点实验室, 包头 014010;

2. 钢铁研究总院 功能材料研究所, 北京 100081

**摘要:** 采用快淬技术制备 Mg<sub>2</sub>Ni 型纳米晶和非晶(Mg<sub>24</sub>Ni<sub>10</sub>Cu<sub>2</sub>)<sub>100-x</sub>Nd<sub>x</sub> (x=0, 5, 10, 15, 20)合金, 研究快淬速度对合金相结构和电化学性能的影响。结果表明, 快淬态无 Nd 合金为纳米晶结构, 而添加 Nd 元素的快淬态合金为纳米晶和非晶结构, 表明添加 Nd 元素可促进 Mg<sub>2</sub>Ni 型合金的非晶形成能力。当快淬速度从 0 增加至 40 m/s 时, x=0 合金的放电容量从 42.5 增加至 100.6 mA·h/g; x=10 合金的放电容量从 86.4 增加至 452.8 mA·h/g。与此同时, x=0 合金的循环稳定性(S<sub>20</sub>)也由 40.2%增加到 41.1%, 而 x=10 合金的 S<sub>20</sub> 值由 53.2%增加到 89.7%。

**关键词:** 贮氢; 合金; Mg<sub>2</sub>Ni 型合金; Nd; 快淬; 相结构

(Edited by Hua YANG)